LIMNOLOGY and OCEANOGRAPHY

ASLO

Limnol. Oceanogr. 69, 2024, 1941–1954

doi: 10.1002/lno.12635

Decoupled cycling of particulate cadmium and phosphorus in the subtropical Northwest Pacific

Kan Zhang, Kuanbo Zhou, Yihua Cai, Zhongwei Yuan, Yaojin Chen, Feipeng Xu, Xin Liu, Zhimian Cao, Minhan Dai*

State Key Laboratory of Marine Environmental Science & College of Ocean and Earth Sciences, Xiamen University, Xiamen, China

Abstract

We examined the spatial variation in size-fractionated (0.8–51 and > 51 μm) particulate cadmium (Cd) and phosphorus (P) based on a large dataset collected during a GEOTRACES Section cruise (GP09) in the North Pacific Subtropical Gyre (NPSG) to better understand the interrelationship between Cd and P biogeochemical cycles. Concentrations of particulate Cd (0.06–2.15 pmol L^{-1}) and P (0.33–10.19 nmol L^{-1}) showed an initial increase with depth followed by a decrease, and were among the lowest observed in the global ocean. Bulk particulate Cd : P ratios in the euphotic zone, indicative of phytoplankton Cd assimilation, showed strong geographic variability averaging 0.05 ± 0.02 within the NPSG interior vs. 0.14 ± 0.04 pmol $nmol^{-1}$ at the southern boundary. Cadmium to P remineralization ratio in the mesopelagic zone had a roughly similar stoichiometry as what was produced in the euphotic zone, being ~ 0.05 ± 0.01 in the NPSG interior vs. 0.21 ± 0.04 pmol $nmol^{-1}$ at the southern boundary. Cd–P decoupling was reflected in the elements' vertical distribution, showing unsynchronized changes through the water column, consistent with Cd–P differential remineralization resulting from multiple Cd and P pools. The Cd–P relationship also differed between small and large particles, suggesting differences in Cd assimilation among phytoplankton assemblages as well as particle dynamic processes. Our results highlight complex processes fractionating Cd from P in the oligotrophic ocean and complicate the use of Cd as a palaeophosphate proxy.

Cadmium (Cd) is an element that is highly toxic to human health but an important micronutrient in the oceans (Xu and Morel 2013). It can serve as a metal cofactor for Cd-carbonic anhydrase (CDCA) in marine diatoms, an enzyme that plays a pivotal role in the acquisition of inorganic carbon for photosynthesis, thus establishing a link between the biogeochemical cycles of carbon and Cd (Lane et al. 2005). In addition, other microalgae that do not possess the CDCA enzyme, including coccolithophores, chlorophytes and several diatom species (Park et al. 2007), may also upregulate their Cd uptake to alleviate zinc (Zn) limitation (Lee and Morel 1995; Sunda and Huntsman 2000; Xu et al. 2007). Cadmium quotas in phytoplankton can be assessed by normalizing Cd to phosphorus (P, a proxy for phytoplankton biomass; Moore et al. 2013) in individual cells or bulk particle assemblages, and have been demonstrated to be highly variable among species and oceanic regions (Ho et al. 2003; Bourne et al. 2018).

Most insights into Cd cycling in the ocean have come from studies of its dissolved distributions. Early data revealed a strong correlation between dissolved Cd and the macronutrient phosphate (PO_4) (e.g., Boyle et al. 1976; Bruland et al. 1978), leading to the use of Cd records preserved in planktonic and benthic foraminifera to reconstruct surface and deep-water phosphate distributions in ancient oceans (Boyle 1988; Elderfield and Rickaby 2000). However, global data compilation has shown that the relationship between dissolved Cd and PO_4 is nonlinear, with a pronounced "kink" occurring at a dissolved PO_4 concentration of ~ 1.3 μmol L^{-1} (Baar et al. 1994; Middag et al. 2018), confounding the use of Cd as an accurate paleonutrient proxy. Recent studies have reached a consensus that mixing between different water masses with different preformed dissolved Cd : PO_4 ratios is the dominant factor explaining the variability in the dissolved Cd and PO_4 relationship (Xie et al. 2015; Middag et al. 2018; Sieber et al. 2023).

*Correspondence: mdai@xmu.edu.cn

Additional Supporting Information may be found in the online version of this article.

Author Contribution Statement: MD conceived and wrote the proposal that funded the research cruise. KZha and KZho led particle sampling with assistance from FX, ZC, and YCa. KZha conducted the particulate trace element analysis assisted by YCh and ZY. XL and FX contributed to the phytoplankton community analysis. KZha interpreted the data and wrote the manuscript. All authors discussed and contributed their comments to the manuscript.

Nonetheless, Cd and P addition via local remineralization could also explain the smaller-scale variability that could not be fully accounted for by thermohaline circulation, most notably in the upper ocean (Quay et al. 2015; Middag et al. 2018; Liu et al. 2022). Furthermore, in high-latitude high nutrient low chlorophyll (HNLC) oceanic regions, the elevated phytoplankton uptake of Cd and subsequent remineralization of high Cd : P particulate matter at depth leave the surface water with a lower dissolved Cd : PO_4 ratio relative to that of deep water (Cullen 2006; Baars et al. 2014). Such particle cycling processes have been suggested to decouple the dissolved Cd and PO_4 distributions at high latitude oceans and in water masses originating there, thus playing a first-order control on the global dissolved Cd–PO_4 relationship (Cullen 2006; Baars et al. 2014; Souza et al. 2022). Therefore, understanding the factors that influence Cd and P assimilation and remineralization in the ocean is vital to clarify local and global dissolved Cd–PO_4 cycling.

However, studies considering the effect of particle cycling have often employed indirect approaches inferred from independent dissolved datasets. For instance, the Cd : P ratio of phytoplankton exported from the euphotic zone can be estimated using the regression slope of dissolved Cd and PO_4 concentrations in the oceanic nutricline, with the assumption that the ocean is at steady-state and that Cd is remineralized to the same extent as P, as described by Lane et al. (2009). Nonetheless, preferential remineralization of P over Cd in shallow waters has been proposed (Bourne et al. 2018), which may affect these estimates. In addition, this approach may be infeasible if the slope is influenced by mixing of water masses with different preformed dissolved Cd : PO_4 ratios and/or different remineralization ratios (Middag et al. 2018). In contrast, studies on changes in Cd and P concentrations in marine particles that incorporate direct information on assimilation, remineralization, aggregation, disaggregation, and scavenging processes remain limited to date (Waeles et al. 2016; Bourne et al. 2018; Lee et al. 2018), especially in the Northwest Pacific (Liao et al. 2017; Yang et al. 2018). Bourne et al. (2018) compiled the euphotic zone Cd : P values in particles collected using large volume in situ filtration systems from the world's oceans, and identified three parameters—dissolved nitrate and silicate concentrations, and euphotic zone depth—to predict how particulate Cd : P varies spatially and temporally. Still, they noted the scarcity of particulate Cd and P data from oligotrophic stations, which hampered accurate predictions for these regions.

Here, we report the first depth profiles of size-fractionated (0.8–51 μm; > 51 μm) particulate Cd and P concentrations in the western sector of the oligotrophic North Pacific Subtropical Gyre (NPSG) from the China GEOTRACES Section GP09. This study aims to quantify Cd : P ratios associated with biological assimilation and organic remineralization in the NPSG, and to provide insight into the mechanisms underlying these features. It also aims to explore the particulate Cd and P cycling through the water column and among different particle size classes in this oligotrophic environment.

Methods

Study area

Samples were collected onboard the RV *Tan Kah Kee* during the China GEOTRACES GP09 cruise from April 25 to June 13, 2019. Sampling stations were located in the western portion of the subtropical North Pacific, spanning three contrasting settings, including (1) the NPSG interior (K2–K6 and K14); (2) the North Equatorial Current (NEC; the southern boundary of the NPSG) that originates in the eastern tropical Pacific (K7–K13); and (3) the upstream Kuroshio Current (KC) that branches off from the NEC (K1) (Fig. 1a). All investigated stations were strongly oligotrophic with nitrate concentrations in surface water mostly below limit of quantitation (< 7.46 nmol L^{-1}) (Browning et al. 2021).

The body of water in the study area, from shallow to deep, is mainly composed of surface water, North Pacific Tropical Water (NPTW), North Pacific Intermediate Water (NPIW), Pacific Deep Water (PDW) and Lower Circumpolar Deep Water (LCDW) (Fig. 1b,c). Detailed hydrographic settings are described in Supporting Information Text S1. The surface mixed layer depth in the study area (~ 30 m) was determined as the depth at which potential density changed by 0.03 kg m^{-3} relative to the near-surface value at 10 m depth (de Boyer Montégut et al. 2004). While the euphotic zone depth (~ 140 m) was determined as the depth at which the photosynthetically active radiation (PAR) was 0.1% of its surface value (Banse 2004).

Sampling of marine particles

Marine particles were sampled using large-volume in situ pumps, following a strict "trace metal clean" GEOTRACES protocol (Cutter et al. 2017). Large particles (> 51 μm) were collected from the 51 μm pore size prefilters, while small particles (0.8–51 μm) were collected from the 0.8 μm pore size Supor® polyethersulfone filters. More details about filter holders, pump deployment and recovery, and particle sample handling are described in Supporting Information Text S2.

Particulate trace element analysis

The analytical method for particulate trace elements was the one used in Xiang and Lam (2020). Briefly, an acid refluxing method using a mixture of hydrofluoric and nitric acids was employed for particle digestion (Cullen and Sherrell 1999; Planquette and Sherrell 2012), followed by detection using sector high-resolution field inductively coupled plasma mass spectrometry (SF-HR-ICP-MS, Element XR Thermo Scientific). Details about the method are given in Supporting Information Text S2. For each digestion batch (~ 40 samples), at least one certified reference material, BCR®-414 (plankton powder), was processed as a sample to assess the accuracy of the methodology. The recoveries for BCR®-414 from 13 separate measurements are presented in Supporting Information Table S2.

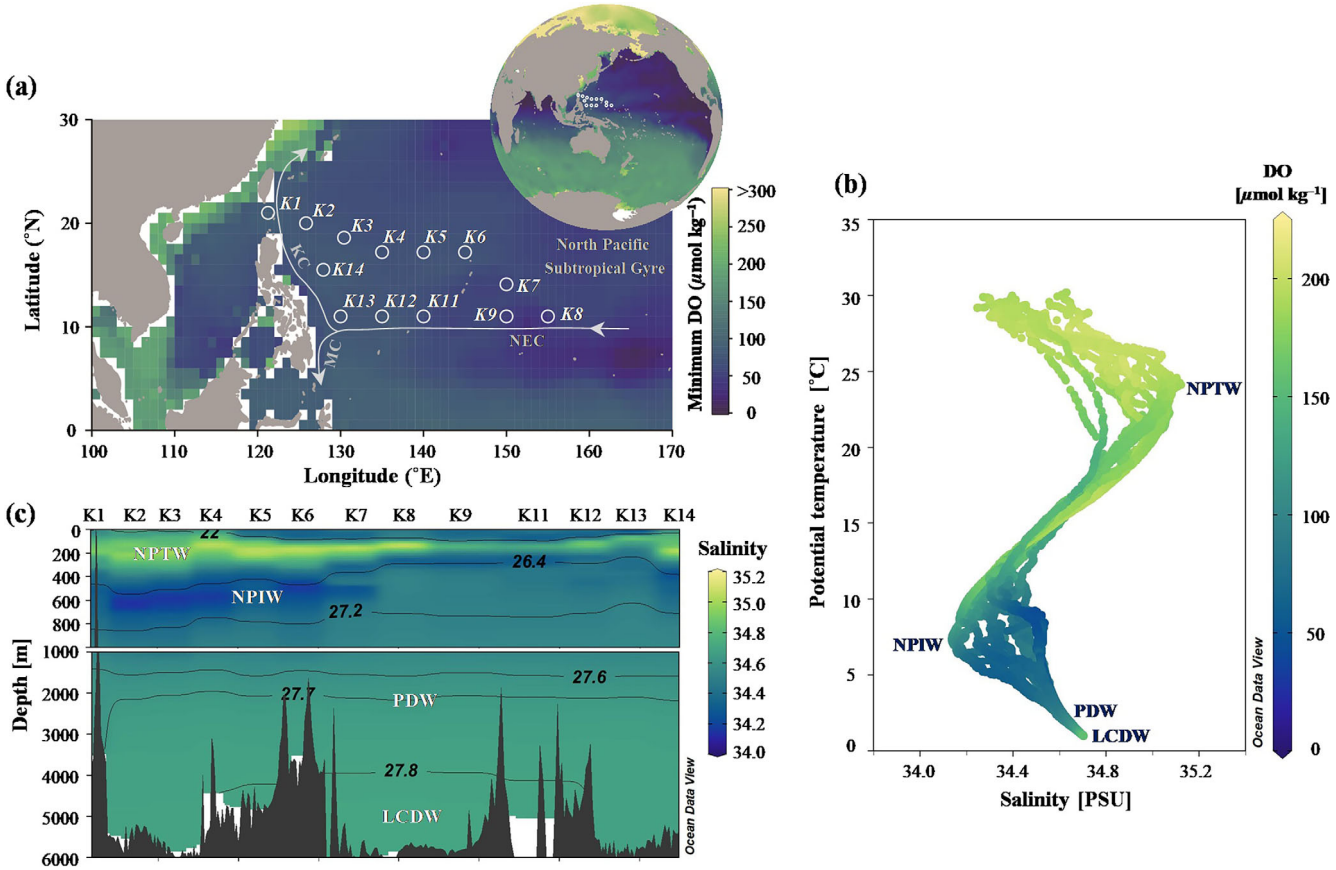

Fig. 1. (**a**) Location of sampling stations (K1–K14) along the GP09 Northwestern Pacific Transect, overlaid with minimum water column dissolved oxygen (DO) concentrations from the 2018 World Ocean Atlas (Boyer et al. 2018). Surface currents are shown as solid lines: North Equatorial Current (NEC), Kuroshio Current (KC), and Mindanao Current (MC). Top global map shows the location of the study area. (**b**) Potential temperature vs. salinity (*T*–*S*) diagram of the sampling stations, color-coded to indicate dissolved oxygen concentrations. (**c**) Salinity depth distribution with potential density anomaly (kg m^{-3}) contours along the GP09 transect. Major water masses based on Talley et al. (2011) are indicated in panels (**b**) and (**c**), including North Pacific Tropical Water (NPTW), North Pacific Intermediate Water (NPIW), Pacific Deep Water (PDW), and Lower Circumpolar Deep Water (LCDW). Panels (**b**) and (**c**) were created using Ocean Data View software (Schlitzer 2020).

Other supporting parameters

Seawater samples (4–8 liters) were filtered onto 25 mm diameter, 0.7 μm pore size Whatman GF/F glass fiber filters for photosynthetic pigment analysis. Pigment concentrations were measured using high performance liquid chromatography (HPLC), and the relative contributions of nine major phytoplankton groups—including dinoflagellates, diatoms, haptophytes_8, haptophytes_6, *Synechococcus*, *Prochlorococcus*, prasinophytes, chlorophytes and cryptophytes—to total chlorophyll *a* (Chl *a*) were calculated using the CHEMTAX approach (Mackey et al. 1996). Samples for both dissolved Fe and PO_4 analysis were collected using a trace-metal-clean rosette with Niskin-X bottles. Dissolved Fe concentrations (filtered through a 0.45 μm pore size capsule filter) were analyzed by chemiluminescence-based flow injection (King et al. 1995) after preconcentration by an inline PA-1 column. Additional details of the analysis were described in Wen et al. (2022). Dissolved PO_4 concentrations were analyzed onboard using a Four-channel Continuous Flow Technicon AA3 Auto-Analyzer (Bran-Lube GmbH) with a quantitation limit (10 times the standard deviation of the blanks) of 0.08 μmol L^{-1}. For samples with dissolved PO_4 concentrations initially detected as below 0.08 μmol L^{-1} via AA3 analysis, nanomolar techniques were applied following Ma et al. (2008).

Results

Total particulate Cd, P concentrations, and Cd : P ratio

The total particulate element concentrations are the sum of small size fraction and large size fraction. The particulate Cd, P concentrations and Cd : P ratio refer to the total ones if not specified. Concentrations of particulate Cd (0.06–2.15 pmol L^{-1}) and P (0.33–10.19 nmol L^{-1}) were among the lowest observed in the global ocean. A comparison with previously reported data collected using the same filter suite is detailed in Supporting Information Text S3.

The particulate Cd depth profiles typically showed a trend of increasing concentrations towards the deep chlorophyll maximum (DCM) layer (~ 120 m) and then decreasing to extremely low values (< 0.1 pmol L^{-1}) at depth (> 1000 m) (Fig. 2a). Obvious spatial differences in particulate Cd concentrations can be observed. The southern stations affected by NEC (K8–K13) had relatively higher particulate Cd concentrations in the upper 500 m water column, with > 0.5 pmol L^{-1} particulate Cd in the surface mixed layer and more pronounced increases towards the DCM layer (the maximum peak value was 2.15 pmol L^{-1}). By contrast, the northern stations away from NEC (K1–K6 and K14) exhibited 0.1–0.2 pmol L^{-1} particulate Cd in the surface mixed layer and slight increases towards the DCM layer (the maximum peak value was 0.58 pmol L^{-1}). Sta. K7, located between the NEC to the south and the NPSG interior to the north, exhibited transitional characteristics with a particulate Cd concentration of 0.46 pmol L^{-1} in the surface mixed layer and a moderate increase toward the DCM layer (the peak value was 0.87 pmol L^{-1}). Particulate P concentrations did not show the same obvious spatial variability as particulate Cd. The particulate P concentrations were overall higher (~ 4–10 nmol L^{-1}) in the upper 100 m water column and then decreased rapidly with increasing depth prior to stabilizing at < 0.5 nmol L^{-1} (Fig. 2b). Peak particulate P concentrations generally occurred at shallower depths than the DCM layer.

The particulate Cd : P ratios ranged from 0.03 to 0.69 pmol $nmol^{-1}$ during the study cruise. Vertically, the particulate Cd : P ratios first increased with depth and then decreased (Fig. 2c). The particulate Cd : P maxima were always found below the euphotic zone and mostly corresponded to the oxycline where the dissolved oxygen concentrations decreased from ~ 175 to 50 μmol kg^{-1} (Fig. 2d). Horizontally, the particulate Cd : P ratios showed a regional gradient as particulate Cd, and striking differences in this ratio occurred mainly in the upper 500 m water column below which the particulate Cd : P profiles gradually overlapped. In the upper 500 m, stations in the NEC (including K7) exhibited higher particulate Cd : P ratios with maxima of 0.46–0.69 pmol $nmol^{-1}$, compared to those further north characterized by maxima of 0.19–0.36 pmol $nmol^{-1}$ (Fig. 2c).

Size-fractionated particulate Cd, P concentrations, and Cd : P ratio

Large particles (> 51 μm) comprised a minor portion of the total. The percentages of particulate Cd occurring in large particles relative to the total were generally less than 25%, except at Stas. K1 and K2 where this percentage increased to ~ 30–35% in the surface mixed layer (Fig. 3d). The percentages of large particulate P were mostly less than 10% (Fig. 3h). Small particulate Cd and P concentrations, as well as Cd : P ratios, exhibited distribution patterns similar to those of total particles (Fig. 3a–c). Large particulate Cd and P concentrations were also higher in the euphotic zone and then decreased with depth (Fig. 3e,f). For the Cd : P ratio in large particles, we focused mainly on the upper 250 m water column since the large particulate P concentrations at depth were mostly below the detection limit (~ 84%), which may generate anomalous Cd : P values. Spatial variability of Cd : P ratio was also observed within large particles (Fig. 3g). And in the euphotic zone, particulate Cd : P ratios were relatively higher in large particles than in the corresponding small particles by a factor of 3.3 ± 1.6 (average ± SD, $n = 46$).

Phytoplankton biomass and community structure

Phytoplankton biomass was inferred from total Chl *a* concentration (TChl *a*), with an average of 66 ± 22 ng L^{-1}

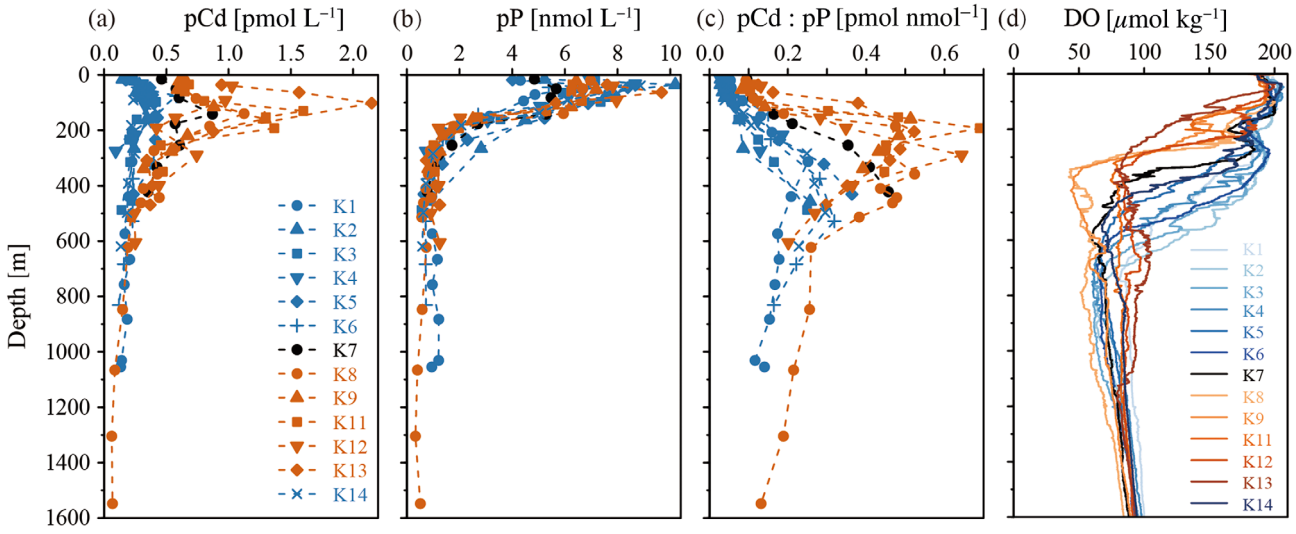

Fig. 2. Depth profiles of (a) total particulate cadmium (pCd), (b) total particulate phosphorus (pP), (c) total particulate Cd : P ratio (pCd : pP), and (d) dissolved oxygen (DO) concentration measured by the SBE 43 DO sensor. The symbols for pP and pCd : pP are the same as pCd.

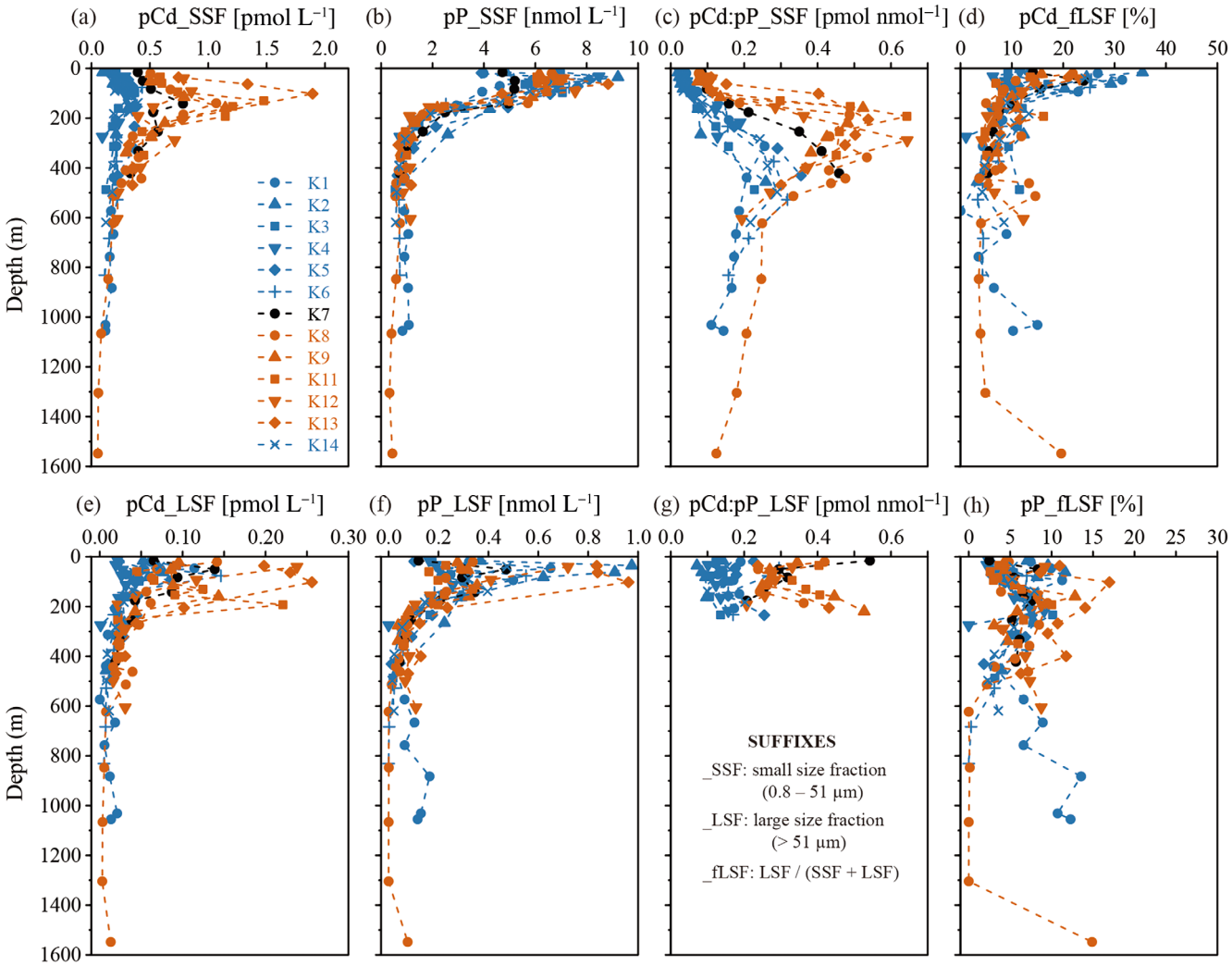

Fig. 3. Depth profiles of (a-c) particulate cadmium (pCd), particulate phosphorus (pP), particulate Cd : P ratio in small size fraction (0.8–51 μm; SSF), (e-g) particulate Cd, particulate P and particulate Cd:P ratio in large size fraction (> 51 μm; LSF), and (d, h) the percentages of Cd and P concentrations occurring in large particles relative to the total (fLSF). Note that the large particulate P concentrations below 250 m were mostly below the detection limit, preventing a meaningful calculation of Cd : P ratio. Thus, the large particulate Cd : P ratios below 250 m are not shown in panel (**g**).

in surface water and 418 ± 76 ng L^{-1} at the DCM layer ($n = 13$). The CHEMTAX results showed that *Synechococcus* and *Prochlorococcus* together contributed ~ 80% of the TChl *a*. Haptophytes_8 is the third major phytoplankton in the study area, contributing ~ 10% of the TChl *a* across most water depths. However, this contribution increased to 20–50% around the base of the euphotic zone (Fig. 4).

Nutrient conditions in the euphotic zone

Depth-integrated averages of dissolved PO_4 and Fe in the euphotic zone were calculated to characterize the ambient nutrient conditions (Fig. 5; Supporting Information Table S3). No clear spatial differences were observed in the dissolved Fe concentrations (average ± SD = 0.23 ± 0.04 nmol L^{-1}, $n = 13$), but the dissolved PO_4 concentrations showed a pronounced gradient, increasing by a factor of ~ 5 from an average of 32.45 ± 8.91 nmol L^{-1} in the northern region (K1–K6 and K14) to 159.26 ± 76.16 nmol L^{-1} in the southern NEC region (K7–K13). Thus, the dissolved Fe : PO_4 ratios decreased ~ fourfolds from an average of 7.61 ± 1.67 nmol μmol^{-1} in the north to 1.76 ± 1.20 nmol μmol^{-1} in the south. In addition, the dissolved PO_4 concentrations and Fe : PO_4 ratios exhibited strong positive ($R^2 = 0.92$, $p < 0.0001$) and negative ($R^2 = 0.86$, $p < 0.0001$) correlations, respectively, with the averaged particulate Cd : P ratios in the euphotic zone (Fig. 6).

The nutrient supply rates into the euphotic zone, from aerosol deposition and turbulent diffusion, were also estimated using methods described in Supporting Information Text S4. In contrast to the indistinguishable dissolved Fe concentrations, the Fe supply rates were higher in the north (8.7 ± 6.6 nmol m^{-2} d^{-1}) and declined in the south (3.8 ± 1.0 nmol m^{-2} d^{-1}), which were mainly resulted from

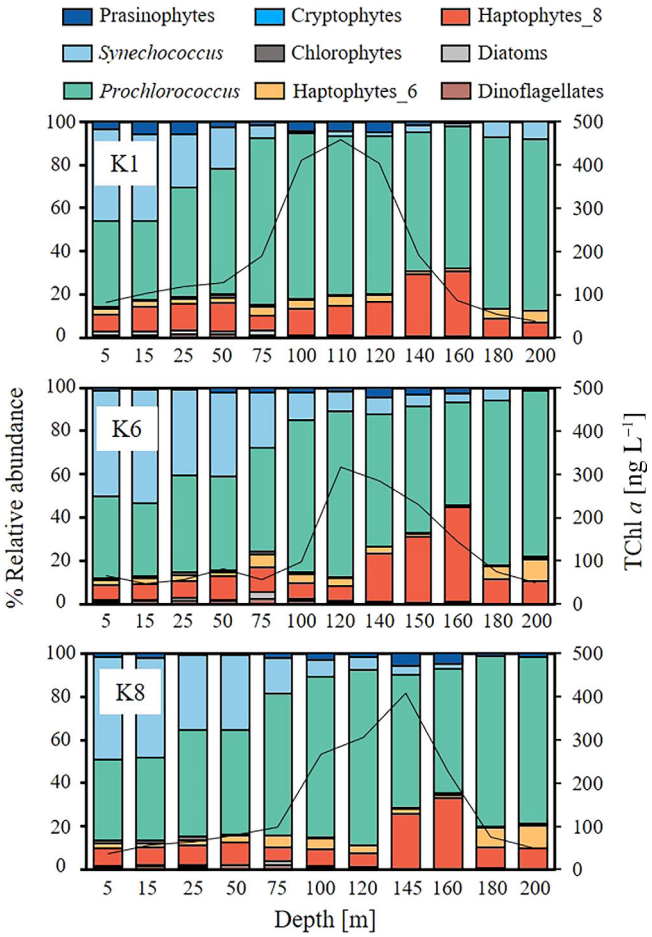

Fig. 4. The total chlorophyll *a* concentration (TChl *a*; black line) and phytoplankton community composition at three representative stations in the subtropical Northwest Pacific. The stations include K1, through which the Kuroshio Current flowed; K6, located in the interior of the North Pacific Subtropical Gyre; and K8, located in the North Equatorial Current affected zone.

the differences in aerosol supply rates from above between these two regions. Similar to the spatial gradient of dissolved PO_4 concentrations, the P supply rates were also lower in the north (1.50 ± 1.27 μmol m^{-2} d^{-1}) and higher in the south (7.84 ± 6.82 μmol m^{-2} d^{-1}), mainly due to the differences in turbulent supply rates from subsurface waters. Thus, the Fe : P supply ratios into the euphotic zone decreased from an average of 290.78 ± 496.96 nmol μmol^{-1} in the north to 0.79 ± 0.55 nmol μmol^{-1} in the south (Fig. 5).

Remineralization ratio of Cd to P in the mesopelagic zone

Microbial remineralization and nutrient recycling predominantly occur in the mesopelagic zone (Saito et al. 2020; Cram et al. 2022). Here, we define "mesopelagic" as the region between the base of the euphotic zone and 1000 m, following Cram et al. (2022). The slope of the regression line between particulate Cd and particulate P in the mesopelagic zone could represent the remineralization ratio of Cd to P as particles degrade (referred to as ΔCd : ΔP), adapted from Lam et al. (2018) for carbon, nitrogen and phosphorus. As shown in Fig. 7, the ΔCd : ΔP was 0.21 ± 0.04 pmol nmol^{-1} ($R^2 = 0.47$, $p < 0.0001$) for Stas. K7–K13 in the NEC region, and 0.05 ± 0.01 pmol nmol^{-1} ($R^2 = 0.54$, $p < 0.0001$) for Stas. K1–K6 and K14 in the NPSG interior and KC.

Discussion

Spatial heterogeneity in phytoplankton Cd assimilation

The particulate Cd and P data obtained via analysis of bulk particulate matter from the euphotic zone can be used to reflect the biochemical demand of phytoplankton, as these elements are primarily associated with biogenic materials and exhibit low adsorption affinity to solid surfaces (Twining and Baines 2013; John and Conway 2014; Zheng et al. 2021). Their lack of correlation with particulate aluminum (Supporting Information Fig. S1), a commonly used lithogenic tracer, further indicates an insignificant contribution from lithogenic matter. Investigating the factors driving the spatial variability in particulate Cd, P and Cd : P is of critical importance for understanding the interactions between environmental conditions and marine algal growth, as well as the biogeochemical cycling of these nutrients in the ocean.

Both particulate Cd concentrations and Cd : P ratios in the study area showed a north–south spatial gradient, with relatively higher values in the NEC (0.92 ± 0.32 pmol L^{-1} and 0.14 ± 0.04 pmol nmol^{-1}, respectively, for the euphotic zone average) compared to those further north in the KC and NPSG interior (0.32 ± 0.05 pmol L^{-1} and 0.05 ± 0.02 pmol nmol^{-1}, respectively) (Fig. 5). Several factors influencing the algal uptake of Cd and algal Cd : P ratios have been identified. Phytoplankton species composition is one of the most important determinants of Cd : P ratios (Ho et al. 2003). Phosphorus-normalized cellular Cd quotas can differ by two orders of magnitude among different marine eukaryotic species under identical culture conditions, with green plastid algae, particularly chlorophytes, having relatively low Cd quotas compared to red plastid superfamilies, for example, diatoms and coccolithophores (Ho et al. 2003). This variation was attributed to environmental selection pressure on components of the photosynthetic apparatus where metal substitutions may have occurred early in the evolution of major eukaryotic phytoplankton phyla (Quigg et al. 2003). In addition, prokaryotic cyanobacteria are expected to have relatively lower Cd quotas than eukaryotic algae (Brand et al. 1986; Saito et al. 2003). Field investigations conducted during the two US-JGOFS equatorial Pacific cruises revealed that particulate Cd : P ratios in the euphotic zone increased from 0.55 to 1.1 pmol nmol^{-1}, corresponding to shifts in the phytoplankton community from *Prochlorococcus* and *Synechococcus* dominance to diatom dominance (Bourne et al. 2018). In our

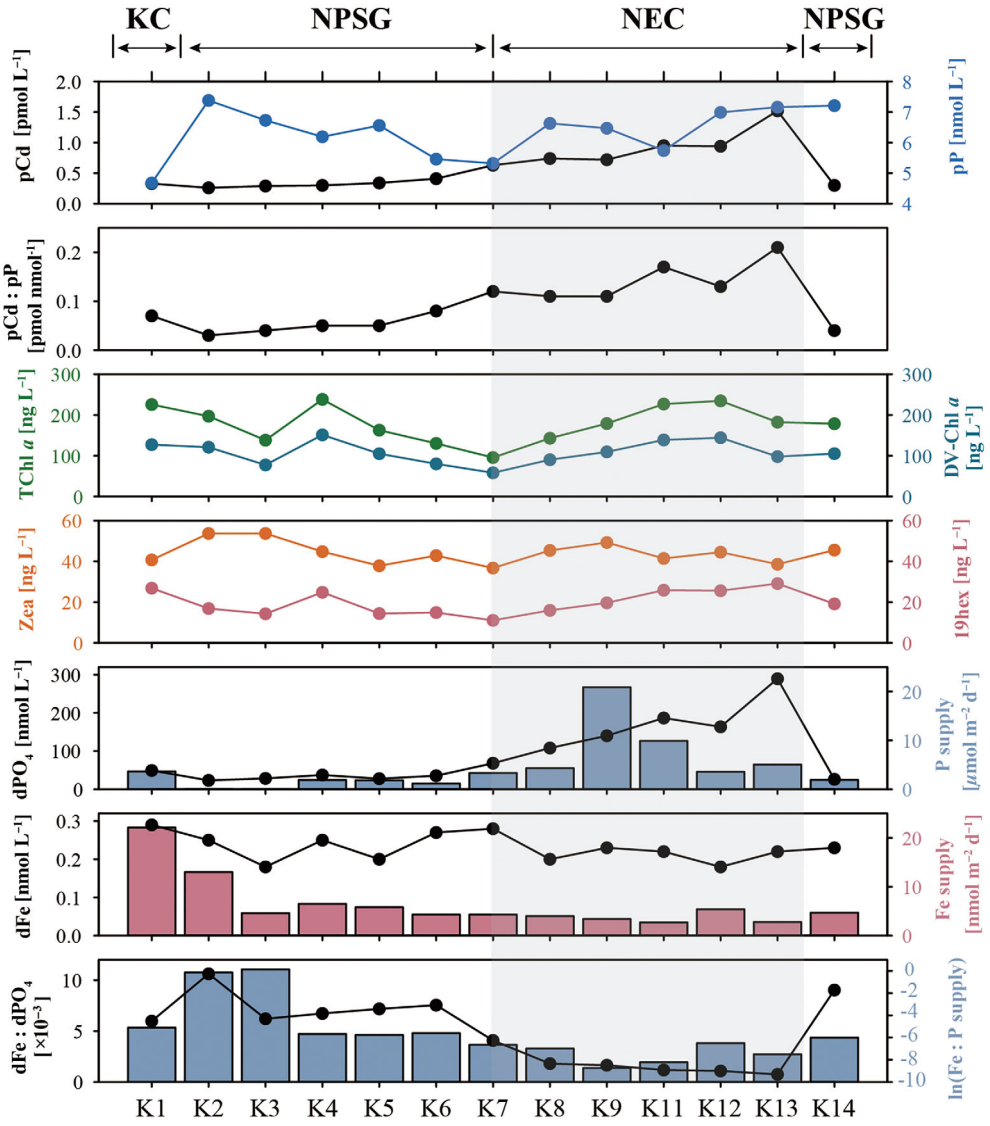

Fig. 5. Particulate, biological, and nutrient conditions at each station during the GP09 cruise. Except for iron (Fe) and phosphorus (P) supply rates from aerosol deposition and turbulent diffusion into the euphotic zone, as well as their supply ratios, other parameters refer to depth-integrated averages over the euphotic zone. Biological parameters include total chlorophyll *a* (TChl *a*) and the main diagnostic photopigments of *Prochlorococcus* (divinyl [DV]-chlorophyll *a*), *Synechococcus* (zeaxanthin) and haptophytes (19-hex-fucoxanthin). The gray shaded area indicates North Equatorial Current (NEC) affected stations.

study area, however, phytoplankton species differences are unlikely to explain the observed spatial variations in particulate Cd and Cd : P, as the main diagnostic photopigments at the investigated sites did not exhibit the same north–south spatial gradient as particulate Cd and Cd : P (Fig. 5). Furthermore, the phytoplankton community structure showed a high degree of consistency among the study sites, being predominantly composed of *Synechococcus* and *Prochlorococcus* (Fig. 4).

A suite of environmental variables can also affect algal Cd uptake. Laboratory and field studies have demonstrated that algal Cd : P ratios are largely dependent on free dissolved Cd concentrations and Cd : PO_4 ratios (Kudo et al. 1996; Middag et al. 2018), and are inversely related to the availability of several essential trace metals, notably Fe, Zn, and manganese (Mn), as well as ambient carbon dioxide partial pressure (Sunda and Huntsman 1998; Cullen and Sherrell 2005). These relationships likely arise from several, not necessarily independent, physiological responses: (1) Cd uptake by nonspecific micronutrient transport systems (e.g., Zn or Mn transport systems) where Cd and other divalent metals compete for binding to uptake sites (Sunda and Huntsman 2000; Kustka et al. 2007); (2) Cd incorporation into the carbonic anhydrase of diatoms as a supplement or substitute for Zn under low Zn conditions (Price and Morel 1990; Lane and Morel 2000);

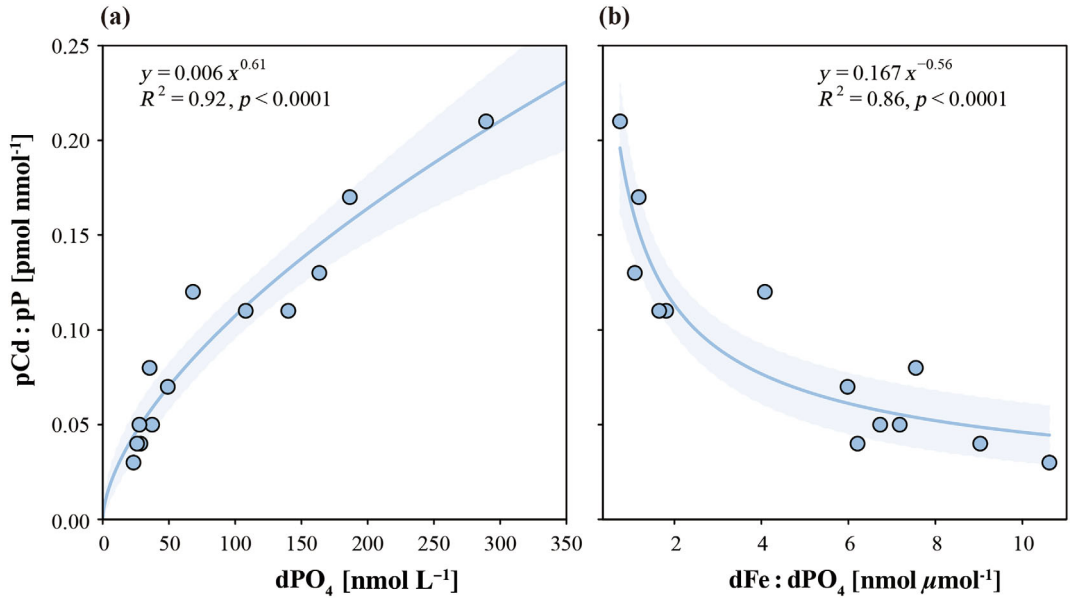

Fig. 6. The particulate cadmium to phosphorus ratio (pCd : pP) as a function of dissolved phosphate concentration (dPO_4) and dissolved iron to phosphate ratio (dFe : dPO_4). Data points represent depth-integrated averages in the euphotic zone at each station during the GP09 cruise. The solid line represents the fitted curvilinear function described by the equation (R^2 = coefficient of determination), with shading around the line indicating the 95% confidence interval.

(3) growth rate dilution, where the Cd uptake rate remains relatively constant while biomass accumulation is limited by Fe availability (Cullen et al. 2003). In our study area, both ambient dissolved Fe and PO_4 concentrations and the supply rates of Fe and P into the euphotic zone indicate reduced Fe availability relative to P in the southern NEC region compared to areas further north (Fig. 5). This finding is consistent with the nitrogen (N)–P–Fe addition experiments conducted during the same cruise, which revealed a geographic shift from primary N limitation in the northern region to N–Fe co-limitation in the southern NEC region (Browning et al. 2021). Such a spatial gradient of nutrient conditions corresponded with that of particulate Cd and Cd : P, suggesting that the higher particulate Cd and Cd : P values in the NEC were likely associated with Fe limitation. Indeed, culture studies on the prokaryotes *Synechococcus* and *Prochlorococcus*, which dominate oligotrophic oceans (Fig. 4), showed an approximate doubling of the cellular Cd : P ratio when grown in Fe-depleted compared to Fe-replete media (Cunningham and John 2017).

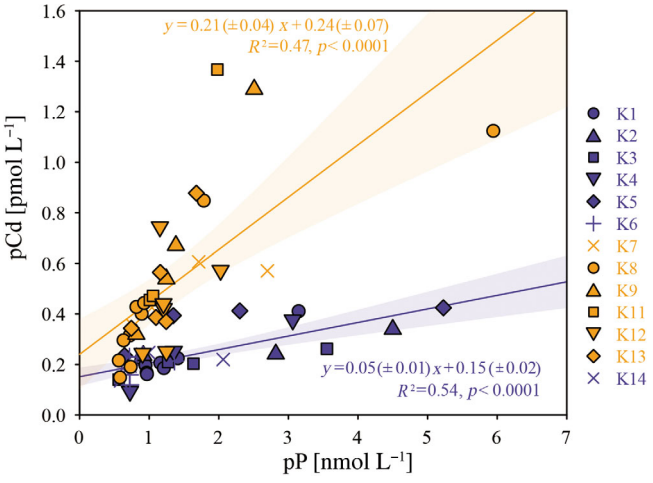

Fig. 7. Particulate cadmium (pCd) vs. particulate phosphorus (pP) concentrations for samples collected from the bottom of the euphotic zone down to 1000 m during the GP09 cruise. The stations were categorized into two groups: K7–K13 in the NEC region (orange) and K1–K6 and K14 in the NPSG interior and KC (purple). The solid line represents the fitted linear regression (R^2 = coefficient of determination), and the shading around the line indicates the 95% confidence interval.

In addition to qualitatively classifying stations in the study area into two broad regions with different Cd quotas, we found that particulate Cd : P ratios generally increased as a power function with increasing dissolved PO_4 concentrations in our samples (Fig. 6a). This trend persisted even when data from the North Atlantic (GEOTRACES GA03 cruise) and South Pacific (GEOTRACES GP16 cruise) were included in the analysis (Supporting Information Fig. S2), despite significant shift in phytoplankton community composition in the Peruvian upwelling region (Twining et al. 2020). The strong correlation between particulate Cd : P and dissolved PO_4 appears to be driven by the depletion of biologically important trace metals (e.g., Fe, Zn) in the presence of elevated macronutrients, given the potential substitution of Cd for other trace metals in some metalloenzymes. Plankton communities appear to be

characterized by a generalizable metal concentration ranking of Fe ≈ Zn > Mn ≈ nickel (Ni) ≈ copper (Cu) ≫ cobalt (Co) ≈ Cd (Twining and Baines 2013). The high biochemical requirement for Fe, combined with its limited supply and low solubility in seawater, leads to Fe limitation across a large portion of the global ocean (Morel et al. 2020). In contrast, the modest requirement for Cd may allow for its sufficient acquisition despite the scarcity of dissolved Cd in the surface ocean (Morel et al. 2020). Data from the GP09, GA03, and GP16 cruises revealed an inverse correlation between particulate Cd : P and dissolved Fe : PO_4 ratios (Fig. 6b; Supporting Information Fig. S2b). Similarly, an inverse correlation was observed between particulate Cd : P ratio and growth rate when examining the effects of Fe limitation on Cd : P composition of natural phytoplankton assemblages through shipboard incubation experiments (Cullen et al. 2003). Hence, our results further demonstrate that Fe deficiency relative to P can increase Cd uptake of natural phytoplankton community, potentially accompanied by a decrease in community growth rate.

Spatial variability in particulate Cd remineralization

Given the extreme plasticity in Cd : P stoichiometry of biological uptake and the differential remineralization rates between Cd and P, a constant addition ratio of Cd to P from organic matter degradation into the dissolved pool is not expected (Souza et al. 2022). Therefore, local remineralization of Cd and P needs to be quantified.

Our results showed significant spatial differences in the remineralization ratio of Cd to P. The ΔCd : ΔP was notably higher in the NEC region (0.21 ± 0.04 pmol nmol^{-1}) compared to the NPSG interior and KC (0.05 ± 0.01 pmol nmol^{-1}) (Fig. 7). These values are comparable to the particulate Cd : P averages in the euphotic zone ($\sim 0.14 \pm 0.04$ and 0.05 ± 0.02 pmol nmol^{-1}, respectively) (Fig. 5), suggesting that the particle pool remineralized in the mesopelagic zone had a roughly similar stoichiometry to what was produced in the euphotic zone. Nonetheless, a steeper slope was observed at low particulate Cd and P concentrations in the NEC region (Fig. 7). This feature became more pronounced when examining individual stations with a relatively high number of data points. For instance, at Sta. K8, the ΔCd : ΔP ratio increased from ~ 0.07 pmol nmol^{-1} above 200 m to ~ 0.70 pmol nmol^{-1} below this depth (Supporting Information Fig. S3). This is consistent with the preferential remineralization of P over Cd in shallow subsurface (Bourne et al. 2018), which results in the remaining particle pool that degrades at depth having a higher ΔCd : ΔP ratio than the euphotic particulate Cd : P ratio. The change in slope also corresponds with the vertical variation of particulate Cd : P ratio, which shifted from increasing to decreasing with depth (Fig. 2c). This trend reversal was hypothesized to result from the preferential remineralization of labile P fractions (such as adenosine triphosphate and nucleotide) over Cd above the particulate Cd : P maximum, and the preferential remineralization of Cd over more refractory P pools (such as phospholipid membranes) below this depth (Bourne et al. 2018). In contrast, the remineralization ratio of Cd to P remained relatively constant in the NPSG interior and KC (Fig. 7; Supporting Information Fig. S3). This stability is likely due to the lower enrichment of particulate Cd produced in the euphotic zone of this region. Although Cd is preferentially remineralized over P at depth, the remaining Cd was too low to result in a significant increase in the ΔCd : ΔP ratio (Fig. 8).

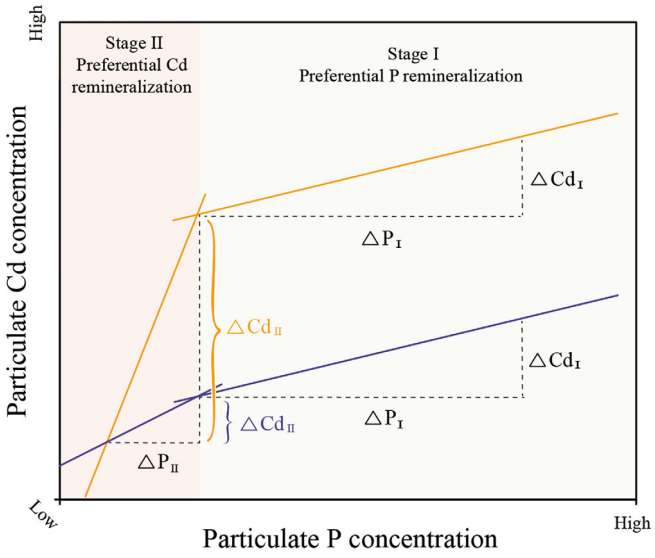

Fig. 8. A schematic diagram illustrating vertical variations in the remineralization ratio of cadmium to phosphorus (ΔCd : ΔP) in the mesopelagic zone across two distinct oceanic regions. The orange and purple lines represent areas characterized by high and low Cd : P stoichiometries of biological uptake, respectively.

Decoupled cycling of Cd and P in the water column

Besides the spatial heterogeneity in the Cd : P ratio of biological uptake and organic remineralization, the vertical profiles of particulate Cd and P concentrations indicate their unsynchronized changes (Fig. 2). As discussed above, a common explanation is provided by the different remineralization rates of Cd vs. P. Furthermore, several other potential mechanisms are considered here.

The structure of the phytoplankton community underwent notable changes with depth. Specifically, the proportion of *Synechococcus*, one of the two dominant autotrophic species, decreased with increasing depth. In contrast, *Prochlorococcus*, the other dominant autotrophic species, exhibited an increase in proportion toward the base of the euphotic zone (Fig. 4). These depth-dependent changes in phytoplankton community composition are often linked to variations in light availability and nutrient concentrations in natural systems (Ryabov et al. 2010). Studies by Cunningham and John (2017)

have shown significant differences in quotas of trace metals including Cd between *Synechococcus* and *Prochlorococcus* and between Fe-delete and Fe-replete conditions. Laboratory experiments have additionally demonstrated that the cyanobacteria species, *Cyanothece* sp., increased its Cd to P ratio under low light conditions (Finkel et al. 2007). Whether *Prochlorococcus*, which adapts to low-light conditions, exhibits a similar increase in the Cd : P ratio remains to be determined. If *Prochlorococcus* does increase its Cd : P ratio under low light, it could contribute to the observed increase in the particulate Cd : P ratio through the euphotic zone. In addition, the proportion of haptophytes, a group of marine eukaryotic phytoplankton, increased near the base of the euphotic zone (Fig. 4). Given that marine eukaryotic phytoplankton are expected to have higher Cd quotas than prokaryotic phytoplankton, a trait thought to be influenced by the ocean's redox state in the early Earth (Quigg et al. 2003; Saito et al. 2003), the increased presence of haptophytes could also contribute to the higher particulate Cd : P ratio observed at this depth. However, to establish a definitive link between the depth-related changes in phytoplankton community composition and the vertical variations in particulate Cd : P ratio, additional direct analysis of the Cd quotas in individual phytoplankton cells collected from various water depths is necessary.

Oceanic Cd cycling may also be influenced by dissolved oxygen levels in the ocean. It has been hypothesized that cadmium sulfide (CdS) precipitation in sulfidic microenvironments within organic particles serves as an important Cd removal mechanism in poorly oxygenated waters (Janssen et al. 2014), although this perspective has been challenged by large-scale datasets afterwards (Xie et al. 2015; Souza et al. 2022). Our study area included a relatively mild oxygen minimum ($\sim$ 42–81 μmol kg^{-1}) at water depths of $\sim$ 350–420 m in the NEC, and $\sim$ 550–840 m in the NPSG interior and KC (Fig. 2d). It is noteworthy that the particulate Cd : P ratios continued to increase below the particulate Cd maximum layer and reached a peak near the base of the upper oxycline (Fig. 2). This layer is generally characterized by a combination of low dissolved oxygen concentration and moderate amount of biogenic particles, thus meeting the two fundamental conditions necessary for the formation of an anoxic microenvironment (Conway and John 2015). However, elevated particulate Cd concentration did not appear with the particulate Cd : P maximum at most stations, suggesting a lack of net transfer of Cd from ambient seawater to particulate phases. Hence, the hypothesis of CdS precipitation within the microenvironment cannot be invoked as an explanation for the particulate Cd : P maxima in this region.

Factors controlling particle size partitioning of Cd and P

Studies on the size partitioning of particulate elements can provide vital information on the size-class dependence of phytoplankton-nutrient interactions (Cullen and Sherrell 1999; Garcia et al. 2016) and particle dynamic processes that link small suspended particles to large sinking particles through particle production, aggregation and disaggregation (Lam et al. 2015; Ohnemus and Lam 2015; Lam et al. 2018). As indicated by the percentage of large particle size fraction relative to the total (Fig. 3d,h), particulate Cd and P were primarily associated with small particles. This is consistent with the phytoplankton community in the study area that was dominated by the small cyanobacteria *Prochlorococcus* and *Synechococcus* (Fig. 4). Although diatoms constituted a minor portion of the total phytoplankton community (Fig. 4), their significance was amplified within the large-sized phytoplankton community. This is supported by the notably high partitioning of diatom-dominated biogenic silicon into the large particle size fraction, averaging 63.8% $\pm$ 12.6% ($n = 62$) in the upper 250 m water column, in contrast to the phytoplankton biomass as indicated by particulate P (Supporting Information Fig. S4).

Considering both laboratory and field studies have demonstrated that Cd enrichment is more prevalent in diatoms than in *Prochlorococcus* and *Synechococcus* (Bourne et al. 2018), the increased relative abundance of diatoms in large particles likely contributes to the elevated particulate Cd : P ratios in large particles compared to their corresponding small particles (Fig. 3c,g). In addition, similar to total particles and small particles, clear spatial variability of Cd : P ratio was also observed within large particles, showing higher values in the NEC region compared to the NPSG interior and KC (Fig. 3g). Despite diatoms being common phytoplankton in large particles, neither their abundance nor their relative proportion in large-sized phytoplankton (indicated by the ratio of biogenic silicon to particulate P) systematically increased in the NEC region compared to areas further north (Supporting Information Fig. S4). Nonetheless, diatoms have been shown to upregulate their Cd uptake under Fe deficiency (Lane et al. 2009), and a negative correlation was observed between the Cd : P ratios in large particles and dissolved Fe : PO_4 ratios (Supporting Information Fig. S5). This suggests that the higher particulate Cd : P ratios in large particles in the NEC region were primarily due to Fe limitation in this area, consistent with our conclusion regarding total particles.

The observed variations in Cd : P ratios between small and large particles in this study are consistent with previous findings in adjacent regions (e.g., east of Taiwan; Liao et al. 2017) and other oligotrophic areas (e.g., Bermuda; Bourne et al. 2018), where cyanobacteria were also the predominant phytoplankton species in the smallest size fraction. Conversely, the HNLC regions (e.g., Subantarctic Zone at $\sim$ 56°S) and some nutrient-replete areas (e.g., Santa Barbara Basin) exhibited higher particulate Cd : P ratios in small particles (< 51 μm) compared to large particles (> 51 μm), despite the majority of particulate Cd and P concentrations also being found in small particles (Bourne et al. 2018). Taking the case of the Subantarctic Zone at $\sim$ 56°S, high levels of haptophytes were observed at this station where most phytoplankton chlorophyll was distributed within the

< 20 μm size fraction (Lance et al. 2007). This suggests that haptophytes dominated the phytoplankton community of small size fraction. Unlike cyanobacteria which dominate in oligotrophic waters and typically have lower Cd quotas, haptophytes appear to possess higher Cd quotas than diatoms (Ho et al. 2003). Therefore, small phytoplankton with higher Cd quotas, for example, haptophytes, are proposed to play a key role in elevating the particulate Cd : P ratios of small particles in HNLC and nutrient-replete regions. In short, the contrasting findings regarding size-fractionated particulate Cd : P ratios observed between oligotrophic waters and other oceanic regions are mainly driven by the composition of phytoplankton assemblages.

Another intriguing difference between small and large particles is their vertical variation of particulate Cd : P ratio in the upper 250 m water column. In contrast to the gradual increase with depth in small particles, the Cd : P ratios in large particles showed a minimum below the surface mixed layer (Fig. 3; Supporting Information Fig. S6). Considering that particle aggregation processes dominate at subsurface layer in a general particle dynamic framework (Lam et al. 2018), we hypothesize that the enhanced aggregation rates of small organic particles into large aggregates may lead to the transfer of low particulate Cd : P signals from small particles to large particles. Oceanic particle dynamics can be inferred from the size partitioning of lithogenic marine particulate trace elements (e.g., Al, Fe, titanium), because the long-distance transport of atmospheric-derived or margin-derived lithogenic materials is likely dominated by fine, suspended particles, and thus the occurrence of lithogenic materials in large particles is a result of aggregation (Lam and Marchal 2015; Ohnemus and Lam 2015). In our study area, the percentage of particulate Al in large particles relative to the total showed a subsurface maximum that is coincident with the minimum of particulate Cd : P in large particles (Supporting Information Fig. S6), supporting the notion of enhanced aggregation processes acting on both lithogenic and biogenic particle phases. Below the subsurface minimum, a gradual increase in large particulate Cd : P ratios may be driven by particle disaggregation, along with other processes such as a preferential release of labile P over Cd.

Conclusions

Size-fractionated (0.8–51 μm; > 51 μm) particulate Cd and P data in the western NPSG illustrate the decoupled cycling of particulate Cd and P, as indicated by spatial variability in their biological uptake and organic remineralization, unsynchronized changes in their vertical distributions, and size-based fractionation. Concentrations of particulate Cd (0.06–2.15 pmol L^{-1}) and P (0.33–10.19 nmol L^{-1}) showed an initial increase with depth followed by a decrease, and were among the lowest observed in the global ocean. Spatially, both particulate Cd concentrations and Cd : P ratios revealed a significant disparity between the NPSG interior and NEC region, highlighting the sensitivity of Cd quota (referred to as particulate Cd : P) as a biological response to insufficient Fe supply (relative to P) in the euphotic zone. Consequently, the ΔCd : ΔP remineralization ratio in the mesopelagic zone exhibited a roughly similar stoichiometry to that produced in the euphotic zone. Vertically, the unsynchronized changes of particulate Cd and P through the water column agree with the differential remineralization rates of multiple Cd and P pools. Depth-related changes in phytoplankton species may also contribute to the vertical variations in particulate Cd : P, while the cadmium sulfide hypothesis was found to be incompatible with observations. In addition, significant differences were observed between small and large particles, including particulate Cd and P primarily partitioned to small particles (typically by > 80%), lower particulate Cd : P ratios in small particles compared to large particles, and a subsurface minimum in the vertical distribution of large particulate Cd : P. These features appear to reflect differences in Cd assimilation among phytoplankton assemblages as well as particle dynamic processes. Future studies integrating dissolved and particulate data are needed to achieve a more comprehensive understanding of Cd and P cycling in the NPSG.

Data availability statement

The particulate cadmium and phosphorus concentration data are available on Science Data Bank (https://doi.org/10.57760/sciencedb.09916, Zhang and Dai 2024).

References

Baar, H. J. W. D., P. M. Saager, R. F. Nolting, and J. V. D. Meer. 1994. Cadmium versus phosphate in the world ocean. Mar. Chem. **46**: 261–281. doi:10.1016/0304-4203(94)90082-5

Baars, O., W. Abouchami, S. J. G. Galer, M. Boye, and P. L. Croot. 2014. Dissolved cadmium in the Southern Ocean: Distribution, speciation, and relation to phosphate. Limnol. Oceanogr. **59**: 385–399. doi:10.4319/lo.2014.59.2.0385

Banse, K. 2004. Should we continue to use the 1% light depth convention for estimating the compensation depth of phytoplankton for another 70 years. Limnol. Oceanogr.: Bull. **13**: 49–52. doi:10.1002/lob.200413349

Bourne, H. L., J. K. B. Bishop, P. J. Lam, and D. C. Ohnemus. 2018. Global spatial and temporal variation of Cd:P in euphotic zone particulates. Glob. Biogeochem. Cycles **32**: 1123–1141. doi:10.1029/2017gb005842

Boyer, T. P., and others. 2018. World Ocean Atlas 2018 [dissolved oxygen]. NOAA National Centers for Environmental Information. Dataset. https://www.ncei.noaa.gov/archive/accession/NCEI-WOA18

Boyle, E. A. 1988. Cadmium: Chemical tracer of deepwater paleoceanography. Paleoceanogr. Paleoclimatol. **3**: 471–489. doi:10.1029/PA003i004p00471

Boyle, E. A., F. Sclater, and J. M. Edmond. 1976. On the marine geochemistry of cadmium. Nature **263**: 42–44. doi:10.1038/263042a0

Brand, L. E., W. G. Sunda, and R. R. L. Guillard. 1986. Reduction of marine phytoplankton reproduction rates by copper and cadmium. J. Exp. Mar. Biol. Ecol. **96**: 225–250. doi:10.1016/0022-0981(86)90205-4

Browning, T. J., and others. 2021. Nutrient co-limitation in the subtropical Northwest Pacific. Limnol. Oceanogr.: Lett. **7**: 52–61. doi:10.1002/lol2.10205

Bruland, K. W., G. A. Knauer, and J. H. Martin. 1978. Cadmium in northeast Pacific waters. Limnol. Oceanogr. **23**: 618–625. doi:10.4319/lo.1978.23.4.0618

Conway, T. M., and S. G. John. 2015. Biogeochemical cycling of cadmium isotopes along a high-resolution section through the North Atlantic Ocean. Geochim. Cosmochim. Acta **148**: 269–283. doi:10.1016/j.gca.2014.09.032

Cram, J. A., and others. 2022. Slow particle remineralization, rather than suppressed disaggregation, drives efficient flux transfer through the eastern tropical North Pacific oxygen deficient zone. Glob. Biogeochem. Cycles **36**: e2021GB007080. doi:10.1029/2021gb007080

Cullen, J. T. 2006. On the nonlinear relationship between dissolved cadmium and phosphate in the modern global ocean: Could chronic iron limitation of phytoplankton growth cause the kink? Limnol. Oceanogr. **51**: 1369–1380. doi:10.4319/lo.2006.51.3.1369

Cullen, J. T., and R. M. Sherrell. 1999. Techniques for determination of trace metals in small samples of size-fractionated particulate matter: Phytoplankton metals off central California. Mar. Chem. **67**: 233–247. doi:10.1016/S0304-4203(99)00060-2

Cullen, J. T., Z. Chase, K. H. Coale, S. E. Fitzwater, and R. M. Sherrell. 2003. Effect of iron limitation on the cadmium to phosphorus ratio of natural phytoplankton assemblages from the Southern Ocean. Limnol. Oceanogr. **48**: 1079–1087. doi:10.4319/lo.2003.48.3.1079

Cullen, J. T., and R. M. Sherrell. 2005. Effects of dissolved carbon dioxide, zinc, and manganese on the cadmium to phosphorus ratio in natural phytoplankton assemblages. Limnol. Oceanogr. **50**: 1193–1204. doi:10.4319/lo.2005.50.4.1193

Cunningham, B. R., and S. G. John. 2017. The effect of iron limitation on cyanobacteria major nutrient and trace element stoichiometry. Limnol. Oceanogr. **62**: 846–858. doi:10.1002/lno.10484

Cutter, G., K. Casciotti, P. Croot, W. Geibert, L.-E. Heimbürger, M. Lohan, H. Planquette, and T. van de Flierdt. 2017. Sampling and sample-handling protocols for GEOTRACES cruises (version 3). GEOTRACES International Project Office. doi:10.25607/OBP-2

de Boyer Montégut, C., G. Madec, A. S. Fischer, A. Lazar, and D. Iudicone. 2004. Mixed layer depth over the global ocean: An examination of profile data and a profile-based climatology. J. Geophys. Res. **109**: C12003. doi:10.1029/2004JC002378

Elderfield, H., and R. E. M. Rickaby. 2000. Oceanic Cd/P ratio and nutrient utilization in the glacial Southern Ocean. Nature **405**: 305–310. doi:10.1038/35012507

Finkel, Z. V., A. S. Quigg, R. K. Chiampi, O. E. Schofield, and P. G. Falkowski. 2007. Phylogenetic diversity in cadmium: Phosphorus ratio regulation by marine phytoplankton. Limnol. Oceanogr. **52**: 1131–1138. doi:10.4319/lo.2007.52.3.1131

Garcia, N. S., J. A. Bonachela, and A. C. Martiny. 2016. Interactions between growth-dependent changes in cell size, nutrient supply and cellular elemental stoichiometry of marine *Synechococcus*. ISME J. **10**: 2715–2724. doi:10.1038/ismej.2016.50

Ho, T. Y., A. Quigg, Z. V. Finkel, A. J. Milligan, K. Wyman, P. G. Falkowski, and F. M. M. Morel. 2003. The elemental composition of some marine phytoplankton. J. Phycol. **39**: 1145–1159. doi:10.1111/j.0022-3646.2003.03-090.x

Janssen, D. J., T. M. Conway, S. G. John, J. R. Christian, D. I. Kramer, T. F. Pedersen, and J. T. Cullen. 2014. Undocumented water column sink for cadmium in open ocean oxygen-deficient zones. Proc. Natl. Acad. Sci. USA **111**: 6888–6893. doi:10.1073/pnas.1402388111

John, S. G., and T. M. Conway. 2014. A role for scavenging in the marine biogeochemical cycling of zinc and zinc isotopes. Earth Planet. Sci. Lett. **394**: 159–167. doi:10.1016/j.epsl.2014.02.053

King, D. W., H. A. Lounsbury, and F. J. Millero. 1995. Rates and mechanism of Fe(II) oxidation at nanomolar total iron concentrations. Environ. Sci. Technol. **29**: 818–824. doi:10.1021/es00003a033

Kudo, I., H. Kokubun, and K. Matsunaga. 1996. Chemical fractionation of phosphorus and cadmium in the marine diatom *Phaeodactylum tricornutum*. Mar. Chem. **52**: 221–231. doi:10.1016/0304-4203(95)00086-0

Kustka, A. B., A. E. Allen, and F. M. M. Morel. 2007. Sequence analysis and transcriptional regulation of iron acquisition genes in two marine diatoms. J. Phycol. **43**: 715–729. doi:10.1111/j.1529-8817.2007.00359.x

Lam, P. J., and O. Marchal. 2015. Insights into particle cycling from thorium and particle data. Annu. Rev. Mar. Sci. **7**: 159–184. doi:10.1146/annurev-marine-010814-015623

Lam, P. J., D. C. Ohnemus, and M. E. Auro. 2015. Size-fractionated major particle composition and concentrations from the US GEOTRACES North Atlantic Zonal Transect. Deep-Sea Res. II: Top. Stud. Oceanogr. **116**: 303–320. doi:10.1016/j.dsr2.2014.11.020

Lam, P. J., J. M. Lee, M. I. Heller, S. Mehic, Y. Xiang, and N. R. Bates. 2018. Size-fractionated distributions of suspended

particle concentration and major phase composition from the U.S. GEOTRACES Eastern Pacific Zonal Transect (GP16). Mar. Chem. **201**: 90–107. doi:10.1016/j.marchem.2017.08.013

Lance, V. P., M. R. Hiscock, A. K. Hilting, D. A. Stuebe, R. R. Bidigare, W. O. Smith Jr., and R. T. Barber. 2007. Primary productivity, differential size fraction and pigment composition responses in two Southern Ocean in situ iron enrichments. Deep-Sea Res. I: Oceanogr. Res. Pap. **54**: 747–773. doi:10.1016/j.dsr.2007.02.008

Lane, T. W., and F. M. M. Morel. 2000. A biological function for cadmium in marine diatoms. Proc. Natl. Acad. Sci. USA **97**: 4627–4631. doi:10.1073/pnas.090091397

Lane, T. W., M. A. Saito, G. N. George, I. J. Pickering, R. C. Prince, and F. M. M. Morel. 2005. A cadmium enzyme from a marine diatom. Nature **435**: 42. doi:10.1038/435042a

Lane, E. S., D. M. Semeniuk, R. F. Strzepek, J. T. Cullen, and M. T. Maldonado. 2009. Effects of iron limitation on intracellular cadmium of cultured phytoplankton: Implications for surface dissolved cadmium to phosphate ratios. Mar. Chem. **115**: 155–162. doi:10.1016/j.marchem.2009.07.008

Lee, J. G., and F. M. M. Morel. 1995. Replacement of zinc by cadmium in marine phytoplankton. Mar. Ecol. Prog. Ser. **127**: 305–309. doi:10.3354/meps127305

Lee, J. M., M. I. Heller, and P. J. Lam. 2018. Size distribution of particulate trace elements in the U.S. GEOTRACES Eastern Pacific Zonal Transect (GP16). Mar. Chem. **201**: 108–123. doi:10.1016/j.marchem.2017.09.006

Liao, W. H., S. C. Yang, and T. Y. Ho. 2017. Trace metal composition of size-fractionated plankton in the Western Philippine Sea: The impact of anthropogenic aerosol deposition. Limnol. Oceanogr. **62**: 2243–2259. doi:10.1002/lno.10564

Liu, T., S. Krisch, R. C. Xie, M. J. Hopwood, M. Dengler, and E. P. Achterberg. 2022. Sediment release in the Benguela upwelling system dominates trace metal input to the shelf and eastern South Atlantic Ocean. Glob. Biogeochem. Cycles **36**: e2022GB007466. doi:10.1029/2022GB007466

Ma, J., D. Yuan, Y. Liang, and M. Dai. 2008. A modified analytical method for the shipboard determination of nanomolar concentrations of orthophosphate in seawater. J. Oceanogr. **64**: 443–449. doi:10.1007/s10872-008-0037-x

Mackey, M. D., D. J. Mackey, H. W. Higgins, and S. W. Wright. 1996. CHEMTAX—A program for estimating class abundances from chemical markers: Application to HPLC measurements of phytoplankton. Mar. Ecol. Prog. Ser. **144**: 265–283. doi:10.3354/meps144265

Middag, R., S. M. A. C. V. Heuven, K. W. Bruland, and H. J. W. D. Baar. 2018. The relationship between cadmium and phosphate in the Atlantic Ocean unravelled. Earth Planet. Sci. Lett. **492**: 79–88. doi:10.1016/j.epsl.2018.03.046

Moore, C. M., and others. 2013. Processes and patterns of oceanic nutrient limitation. Nat. Geosci. **6**: 701–710. doi:10.1038/NGEO1765

Morel, F. M. M., P. J. Lam, and M. A. Saito. 2020. Trace metal substitution in marine phytoplankton. Annu. Rev. Earth Planet. Sci. **48**: 491–517. doi:10.1146/annurev-earth-053018-060108

Ohnemus, D. C., and P. J. Lam. 2015. Cycling of lithogenic marine particles in the US GEOTRACES North Atlantic Transect. Deep-Sea Res. II: Top. Stud. Oceanogr. **116**: 283–302. doi:10.1016/j.dsr2.2014.11.019

Park, H., B. Song, and F. M. M. Morel. 2007. Diversity of the cadmium-containing carbonic anhydrase in marine diatoms and natural waters. Environ. Microbiol. **9**: 403–413. doi:10.1111/j.1462-2920.2006.01151.x

Planquette, H., and R. M. Sherrell. 2012. Sampling for particulate trace element determination using water sampling bottles: Methodology and comparison to in situ pumps. Limnol. Oceanogr.: Methods **10**: 367–388. doi:10.4319/lom.2012.10.367

Price, N. M., and F. M. M. Morel. 1990. Cadmium and cobalt substitution for zinc in a marine diatom. Nature **344**: 658–660. doi:10.1038/344658a0

Quay, P., J. Cullen, W. Landing, and P. Morton. 2015. Processes controlling the distributions of Cd and PO_4 in the ocean. Glob. Biogeochem. Cycles **29**: 830–841. doi:10.1002/2014gb004998

Quigg, A., and others. 2003. The evolutionary inheritance of elemental stoichiometry in marine phytoplankton. Nature **425**: 291–294. doi:10.1038/nature01953

Ryabov, A. B., L. Rudolf, and B. Blasius. 2010. Vertical distribution and composition of phytoplankton under the influence of an upper mixed layer. J. Theor. Biol. **263**: 120–133. doi:10.1016/j.jtbi.2009.10.034

Saito, M. A., D. M. Sigman, and F. M. M. Morel. 2003. The bioinorganic chemistry of the ancient ocean: The co-evolution of cyanobacterial metal requirements and biogeochemical cycles at the Archean–Proterozoic boundary? Inorg. Chim. Acta **356**: 308–318. doi:10.1016/s0020-1693(03)00442-0

Saito, M. A., and others. 2020. Abundant nitrite-oxidizing metalloenzymes in the mesopelagic zone of the tropical Pacific Ocean. Nat. Geosci. **13**: 355–362. doi:10.1038/s41561-020-0565-6

Schlitzer, R. 2020. Ocean data view. http://odv.awi.de

Sieber, M., and others. 2023. Biological, physical, and atmospheric controls on the distribution of cadmium and its isotopes in the Pacific Ocean. Glob. Biogeochem. Cycles **37**: e2022GB007441. doi:10.1029/2022gb007441

Souza, G. F. D., D. Vance, M. Sieber, T. M. Conway, and S. H. Little. 2022. Re-assessing the influence of particle-hosted sulphide precipitation on the marine cadmium cycle. Geochim. Cosmochim. Acta **322**: 274–296. doi:10.1016/j.gca.2022.02.009

Sunda, W. G., and S. A. Huntsman. 1998. Control of Cd concentrations in a coastal diatom by interactions among free ionic Cd, Zn, and Mn in seawater. Environ. Sci. Technol. **32**: 2961–2968. doi:10.1021/es980271y

Sunda, W. G., and S. A. Huntsman. 2000. Effect of Zn, Mn, and Fe on Cd accumulation in phytoplankton: Implications for oceanic Cd cycling. Limnol. Oceanogr. **45**: 1501–1516. doi:10.4319/lo.2000.45.7.1501

Talley, L. D., G. L. Pickard, W. J. Emery, and J. H. Swift. 2011. Pacific Ocean, p. 303–362. *In* Descriptive physical oceanography: An introduction, 6th ed. Academic Press. doi:10.1016/B978-0-7506-4552-2.10010-1

Twining, B. S., and S. B. Baines. 2013. The trace metal composition of marine phytoplankton. Annu. Rev. Mar. Sci. **5**: 191–215. doi:10.1146/annurev-marine-121211-172322

Twining, B. S., and others. 2020. Taxonomic and nutrient controls on phytoplankton iron quotas in the ocean. Limnol. Oceanogr.: Lett. **6**: 96–106. doi:10.1002/lol2.10179

Waeles, M., and others. 2016. Cadmium in the waters off South Morocco: Nature of particles hosting Cd and insights into the mechanisms fractionating Cd from phosphate. J. Geophys. Res.: Oceans **121**: 3106–3120. doi:10.1002/2016JC011688

Wen, Z., and others. 2022. Nutrient regulation of biological nitrogen fixation across the tropical western North Pacific. Sci. Adv. **8**: eabl7564. doi:10.1126/sciadv.abl7564

Xiang, Y., and P. J. Lam. 2020. Size-fractionated compositions of marine suspended particles in the western Arctic Ocean: Lateral and vertical sources. J. Geophys. Res.: Oceans **125**: e2020JC016144. doi:10.1029/2020JC016144

Xie, R. C., S. J. G. Galer, W. Abouchami, M. J. A. Rijkenberg, J. D. Jong, H. J. W. D. Baar, and M. O. Andreae. 2015. The cadmium–phosphate relationship in the western South Atlantic—The importance of mode and intermediate waters on the global systematics. Mar. Chem. **177**: 110–123. doi:10.1016/j.marchem.2015.06.011

Xu, Y., D. Tang, Y. Shaked, and F. M. M. Morel. 2007. Zinc, cadmium, and cobalt interreplacement and relative use efficiencies in the coccolithophore *Emiliania huxleyi*. Limnol. Oceanogr. **52**: 2294–2305. doi:10.4319/lo.2007.52.5.2294

Xu, Y., and F. M. M. Morel. 2013. Cadmium in marine phytoplankton, p. 509–526. *In* A. Sigel, H. Sigel, and R. K. O. Sigel [eds.], Cadmium: From toxicity to essentiality. Metal ions in life sciences, v. **11**. Springer. doi:10.1007/978-94-007-5179-8_16

Yang, S.-C., J. Zhang, Y. Sohrin, and T.-Y. Ho. 2018. Cadmium cycling in the water column of the Kuroshio-Oyashio extension region: Insights from dissolved and particulate isotopic composition. Geochim. Cosmochim. Acta **233**: 66–80. doi:10.1016/j.gca.2018.05.001

Zheng, L., T. Minami, S. Takano, T.-Y. Ho, and Y. Sohrin. 2021. Sectional distribution patterns of Cd, Ni, Zn, and Cu in the North Pacific Ocean: Relationships to nutrients and importance of scavenging. Glob. Biogeochem. Cycles **35**: e2020GB006558. doi:10.1029/2020gb006558

Acknowledgments

This study was funded by the National Natural Science Foundation of China (Grant nos. 42188102, 41890804 to Minhan Dai, and no. 42006045 to Kan Zhang) and the China Postdoctoral Science Foundation (Grant no. 2019M662235 and BX20190182 to Kan Zhang). The authors thank the captain, crew, and scientists of the RV *Tan Kah Kee*. They are also grateful to Phoebe J. Lam, Yang Xiang, Jong-Mi Lee, and Allison Laubach for their meticulous guidance during in situ pump sampling and laboratory analysis of particulate trace elements. They thank Lifang Wang, Jing Liu, and Yaqian Zhou for analysis of dissolved phosphate and iron concentrations. Junhui Chen, Liguo Guo, Weifang Chen, Yifan Ma, Yating Li, Yuye Han, Bei Zhou, Pingping Zhang, and Dongjian Ci are thanked for their assistance in sample collection and/or data processing. They thank Zhe Wang, Yanping Xu, Feifei Meng, Yan Yang, and Xiaoli Ding for their logistical assistance. The authors would also like to thank the editors and reviewers for their constructive comments and suggestions that have improved the paper.

Conflict of Interest

None declared.

Submitted 29 August 2023
Revised 24 February 2024
Accepted 05 July 2024

Associate editor: Vanessa Hatje